The RNA binding protein Npl3 promotes resection of DNA double-strand breaks by regulating the levels of Exo1

Chiara Vittoria Colombo[†], Camilla Trovesi[†], Luca Menin, Maria Pia Longhese[*] and Michela Clerici[*]

Dipartimento di Biotecnologie e Bioscienze, Università di Milano-Bicocca, 20126 Milano, Italy

ABSTRACT

Eukaryotic cells preserve genome integrity upon DNA damage by activating a signaling network that promotes DNA repair and controls cell cycle progression. One of the most severe DNA damage is the DNA double-strand break (DSB), whose 5′ ends can be nucleolitically resected by multiple nucleases to create 3′-ended single-stranded DNA tails that trigger DSB repair by homologous recombination. Here, we identify the *Saccharomyces cerevisiae* RNA binding protein Npl3 as a new player in DSB resection. Npl3 is related to both the metazoan serine-arginine-rich and the heterogeneous nuclear ribonucleo-proteins. *NPL3* deletion impairs the generation of long ssDNA tails at the DSB ends, whereas it does not exacerbate the resection defect of *exo1Δ* cells. Furthermore, either the lack of Npl3 or the inactivation of its RNA-binding domains causes decrease of the exonuclease Exo1 protein levels as well as generation of unusual and extended *EXO1* RNA species. These findings, together with the observation that *EXO1* overexpression partially suppresses the resection defect of *npl3Δ* cells, indicate that Npl3 participates in DSB resection by promoting the proper biogenesis of *EXO1* mRNA.

INTRODUCTION

Eukaryotic cells deal with DNA damage through a multifaceted cellular response, known as DNA damage response (DDR), which promotes DNA repair and couples it with cell cycle progression (1). DNA double-strand breaks (DSBs) are among the most severe lesions. DSBs can be repaired by either non-homologous end-joining (NHEJ), which directly rejoins together the two broken ends, or homologous recombination (HR) that uses intact homologous duplex DNA sequences as a template for accurate repair (2).

HR is promoted by the nucleolytic degradation of the 5′ DSB ends (a process referred to as resection) to yield 3′ single-stranded DNA (ssDNA) tails that invade the homologous duplex and prime reparative DNA synthesis (2). DSB resection is a two-step process that involves multiple nucleases and helicases. A protein complex, which is called MRX (Mre11–Rad50–Xrs2) in the budding yeast *Saccharomyces cerevisiae* and MRN (Mre11–Rad50–Nbs1) in mammals, initiates resection together with the Sae2/CtIP protein by catalyzing an endonucleolytic cleavage of the 5′-terminated DNA strands. This cleavage creates a substrate for two partially overlapping pathways, which depend on the nucleases Exo1 and Dna2, respectively, and promote the generation of long ssDNA tails (reviewed in 3,4). While Exo1 is a 5′-3′ exonuclease capable of efficiently degrading the 5′ end on duplex DNA, the endonuclease Dna2 requires the helicase activity of Sgs1 (orthologue of mammalian BLM) to efficiently remove small fragments from DNA ends (3,4).

DSB end degradation is tightly controlled by both positive and negative regulators, which tune the action of specific resection factors. While the cyclin-dependent kinase (Cdk1 in yeast)-Clb complexes stimulate the activities of both Sae2 and Dna2, the Ku complex and Rad9 inhibit the action of Exo1 and Sgs1-Dna2, respectively (3–5). Exo1 action is also inhibited through phosphorylation by the checkpoint kinase Rad53 (6) and regulated by the ssDNA-binding complex Replication Protein A (RPA), which promotes Exo1 action *in vivo*, and limits Exo1-dependent degradation by increasing Exo1 turnover at DNA ends *in vitro* (7,8). Given the efficiency of Exo1 exonuclease (8), these multiple controls on its action can be important to prevent excessive DNA degradation that could lead to genome instability.

DSB repair is coupled with cell cycle progression by a checkpoint pathway, whose key players are the protein ki-

nases Mec1 and Tel1, orthologs of mammalian ATR and ATM, respectively [1]. While Tel1 is recruited to blunt or minimally processed DNA ends through interaction with MRX [9], Mec1 and its interactor Ddc2 (ATRIP in mammals) are activated by extended RPA-coated ssDNA that is produced by resection [10]. Once activated, Mec1 and Tel1 propagate the checkpoint signal to the effector kinases Rad53 and Chk1 (Chk2 and Chk1 in mammals, respectively), whose activation requires the adaptor Rad9 (53BP1 in mammals) and leads to temporarily arrest cell cycle progression [1].

Increasing evidence suggests the existence of intimate connections between RNA metabolism, DDR and genome integrity [11]. Pre-mRNA molecules are co-transcriptionally processed by the addition of both a 5′-methylguanosine cap and a 3′ poly(A) tail, and eventually spliced before they are exported to the cytoplasm and translated. These events are mediated by RNA-binding proteins (RBPs), most of which belong to the conserved protein families of heterogeneous nuclear ribonucleo-proteins (hnRNPs) and mammalian serine-arginine-rich (SR) proteins [11]. RBPs also protect mRNAs from degradation and contribute to quality control systems that recognize and target to degradation improperly processed mRNAs [12,13]. In eukaryotes, mRNAs are mainly degraded either by the exosome multi-subunit complex, which includes both endo- and 3′-5′ exoribonuclease activities, or by the Xrn family of 5′-3′ exoribonucleases [13,14].

In both yeast and mammals, several RBPs participate to the DDR and the stress response. Many of these RBPs bind to nascent transcripts and prevent transcription-associated genome instability by packaging pre-mRNAs into ribonucleoprotein particles. This packaging limits the generation of DNA:RNA hybrids, which could induce replication stress and DNA damage by interfering with the progression of DNA replication forks (reviewed in [11,15]). Factors involved in RNA metabolism play also more direct roles in the DDR by either recruiting DDR proteins to the site of damage or regulating the expression of repair and checkpoint genes at different levels [11]. Finally, the conserved nonsense-mediated decay (NMD) pathway was recently found to limit HR in *S. cerevisiae* undamaged cells by controlling the transcript and protein levels of HR factors [16].

One of the most abundant *S. cerevisiae* RBPs is Npl3, which shares structural homologies with both SR and hnRNPs protein families, as it possesses two conserved RNA-recognition motifs (RRMs) and a serine- and arginine-rich C-terminal domain [17]. Npl3 is recruited to transcribed regions through the interaction with RNA polymerase II [18,19], and participates in pre-mRNA processing and packaging as well as in mRNA export and translation [12]. Npl3 accumulates at the 3′ end of transcribed genes [20] and seems to play a role in transcription termination, although this role is somehow controversial. In fact, studies with reporter constructs indicated that Npl3 prevents both early transcription termination and recognition of polyadenylation cryptic sites by competing with polyadenylation/termination factors [18,21,22]. However, recent genome-wide analyses showed significant termina-

tion defects in the absence of Npl3, suggesting that Npl3 promotes transcription termination [23].

Similar to other RBPs, Npl3 prevents transcription-associated genome instability by limiting the accumulation of DNA:RNA hybrids [20]. Interestingly, several findings suggest additional Npl3 functions in the DDR. In particular, cells lacking Npl3 are highly sensitive to DSB-inducing agents [20] and to the expression of the EcoRI endonuclease [24]. Furthermore, Npl3 shows negative genetic interactions with the MRX complex [25], and Npl3 inactivation increases the sensitivity of *rad52* or *ku* mutants to genotoxic agents [20]. Finally, checkpoint-dependent Npl3 phosphorylation after methyl methanesulfonate (MMS) treatment suggests that Npl3 activity may be regulated in response to DNA damage [26].

Here, we show that Npl3 promotes both checkpoint activation and the generation of long ssDNA tails at the DSB ends. These functions are at least partially linked to the regulation of Exo1 abundance through the control of *EXO1* mRNA biogenesis. Altogether, our results identify a new function of Npl3 in the response to DSBs and contribute to define the role of this multifunctional RBP in preserving genome stability.

MATERIALS AND METHODS

Yeast strains and media

Strain genotypes are listed in Supplementary Table S1. All the strains are derivatives of JKM139 strain, which was kindly provided by J. Haber (Brandeis University, Waltham, MA, USA). The centromeric plasmid carrying the *tetO-RNH1* allele [27] and the control vector were kindly provided by A. Aguilera (University of Seville, Sevilla, Spain); the *EXO1* 2μ plasmid [28] and the control vector by E. Alani (Cornell University, New York, NY, USA); the control vector and the centromeric plasmids carrying the wild type *NPL3* or the mutant alleles *npl3-F160L*, *npl3-SNK* (*L225S, G241N, E244K*), and *npl3-LSNK* (*F160L, L225S, G241N, E244K*) [29] by J. Lee-Soety (Saint Joseph's University, Philadelphia, PA, USA). Gene deletions and gene tagging were obtained by one-step PCR methods. Cells were grown in YEP medium (1% yeast extract, 2% peptone) supplemented with 2% glucose (YEPD) or 2% raffinose (YEPR). 3% galactose was added to YEPR-growing cells to induce HO expression (YEPRG). The HO-cut efficiency was evaluated after quantitative PCR (qPCR) with a primer pair that overlaps the HO cut site and gives rise a product only when the locus is uncut, and primers at the *TRP3* locus as a control. The cleavage efficiency was calculated by dividing the difference between the values of the HO-specific product calculated with the ΔCt method before and two hours after galactose addition to the value of the HO-specific product before induction.

DSB resection

DSB end resection was analyzed on alkaline agarose gels by using a single-stranded RNA probe complementary to the unresected DSB strand as described in [30]. This probe was obtained by *in vitro* transcription using Promega Riboprobe System-T7 and plasmid pML514 containing a 900-

bp fragment of the *MAT* locus (coordinates 200 870 to 201 587 on chromosome III) as a template. Quantitative analysis of DSB resection was performed by calculating the ratio of band intensities for ssDNA to total amount of DSB products. The resection efficiency was normalized with respect to the HO cleavage efficiency by subtracting the value of the uncut band from the total amount of DSB products for each time point.

Quantitative reverse transcriptase PCR (qRT-PCR)

Total RNA was prepared with the Bio-Rad Aurum total RNA mini kit. First strand cDNA was synthetized with the Bio-Rad iScript™ cDNA Synthesis Kit. After qRT-PCR on a MiniOpticon Real-time PCR system (Bio-Rad), *EXO1* RNA levels were quantified using the $\Delta\Delta$Ct method and normalized to *ALG9* RNA levels. Primer sequences are listed in Supplementary Table S2.

Northern blot

Total RNA was resolved on a 1% agarose gel in formaldehyde gel running buffer (2.2 M formaldehyde, 20 mM MOPS pH 7.0, 8 mM sodium acetate, 1 mM EDTA pH 8.0). The gel was stained with ethidium bromide to detect 18S and 25S ribosomal RNA and then transferred on a nitrocellulose filter. A BamHI–BglII DNA fragment (1437 bp) internal to the *EXO1* coding sequence (+628 to + 2065 from the ATG initiation codon) was extracted from pML546 plasmid, labeled with [α-32P]-dATP by random priming, and used as a probe. pML546 was constructed by inserting a 3109 bp XhoI–NotI blunt fragment containing the *EXO1* gene from pEAm67 2μ plasmid (28) into the SalI-SmaI YEpLac195 vector (31).

5′ rapid amplification of cDNA ends (RACE)

5 μg of total RNA was subjected to reverse transcription using SuperScript™ II (Invitrogen) and an *EXO1* specific primer to obtain the *EXO1* 5′ partial cDNA ends. After RNA degradation with RNaseH1 and poly(A) tailing of the ss-cDNA, a second DNA strand was synthetized starting from a Q_T (Q_{TOTAL}) primer containing both an oligo-dT sequence capable of annealing with the appended poly(A) tail and a unique sequence. The resulting cDNA was used as a template for two subsequent rounds of amplification using primers that anneal to the Q_T sequence and *EXO1* specific primers. The PCR products were run on 1.5% agarose gels and visualized with ethidium bromide. Primer sequences are listed in Supplementary Table S2.

ChIP analysis

ChIP analysis was performed as previously described (32). Chromatin extracts from both *NPL3-HA* and *NPL3* strains were immunoprecipitated with anti-HA antibodies. Input and immunoprecipitated DNA were purified and analyzed by qPCR. Data are expressed as fold enrichment at the HO-induced DSB over that at the non-cleaved *ARO1* locus, after normalization of ChIP signals to the corresponding input for each time point. Fold enrichment was then normalized to the efficiency of DSB induction.

Other techniques

Flow cytometric DNA analysis was determined on a Becton-Dickinson FACScan. Rad53 was detected by using anti-Rad53 polyclonal antibodies (AB104232) from Abcam. Anti-Rfa2 and anti-Rad9 polyclonal antibodies were kindly provided by B. Stillman (Cold Spring Harbor Laboratory, Cold Spring Harbor, NY, USA) and N. Lowndes (University of Ireland, Galway, Ireland), respectively. Quantitative analysis of phosphorylation normalized to the cut efficiency was performed by calculating the ratio of band intensities for slowly-migrating bands to the total amount of protein, and dividing the obtained values by the cleavage efficiency evaluated by qPCR.

RESULTS

Npl3 promotes the activation of a Mec1-dependent checkpoint

The hypersensitivity of *npl3* mutant cells to DSB-inducing agents (20,24) suggests that Npl3 is involved in the response to DSBs. To explore further this hypothesis, we asked whether the lack of Npl3 affects the checkpoint response to a single DSB that is generated by the HO endonuclease, whose gene is expressed from a galactose-inducible promoter in JKM139 haploid cells (33). Galactose addition to these cells induces the generation at the *MAT* locus of a single DSB that cannot be repaired by HR because the homologous donor loci *HML* and *HMR* are deleted (33). This HO-induced DSB triggers a Mec1-dependent checkpoint that causes a G2/M cell cycle arrest, as well as the phosphorylation of both the checkpoint effector kinase Rad53 and the Mec1 interactor Ddc2 (34–36). We analyzed cell cycle progression and phosphorylation of Rad53 and Ddc2 after the induction of a single irreparable DSB in wild type and *npl3Δ* cells carrying a fully functional Ddc2-HA tagged variant. The cleavage efficiency was evaluated by quantitative PCR (qPCR) at the HO cut site 2 h after galactose addition. Cells carrying the deletion of *MEC1* and kept viable by the lack of the ribonucleotide reductase inhibitor Sml1 were used as a control (37).

When G1-arrested cell cultures were spotted on galactose-containing plates, wild type cells arrested as large-budded cells for at least 8 hours after HO induction, while *mec1Δ sml1Δ* cells, which are unable to activate the checkpoint, formed microcolonies with more than two cells within 4–6 hours (Figure 1A). Although the cleavage efficiency was reduced to 82% in *npl3Δ* cells compared to wild type (95%), 60% of *npl3Δ* cells formed microcolonies 8 hours after HO induction, when >80% wild type cells were still arrested (Figure 1A), indicating that Npl3 contributes to arrest the cell cycle in response to an irreparable DSB.

Rad53 and Ddc2 phosphorylation, which causes decreased electrophoretic mobility of the proteins, was analyzed by western blot of comparable amounts of protein extracts (Supplementary Figure S1) after galactose addition to cell cultures exponentially growing in raffinose. As the HO cleavage efficiency was reduced in *npl3Δ* cells compared to wild type (85% versus 97%), we also performed quantitative analyses of Rad53 and Ddc2 phosphorylation by calculating the ratio of slowly-migrating phospho-
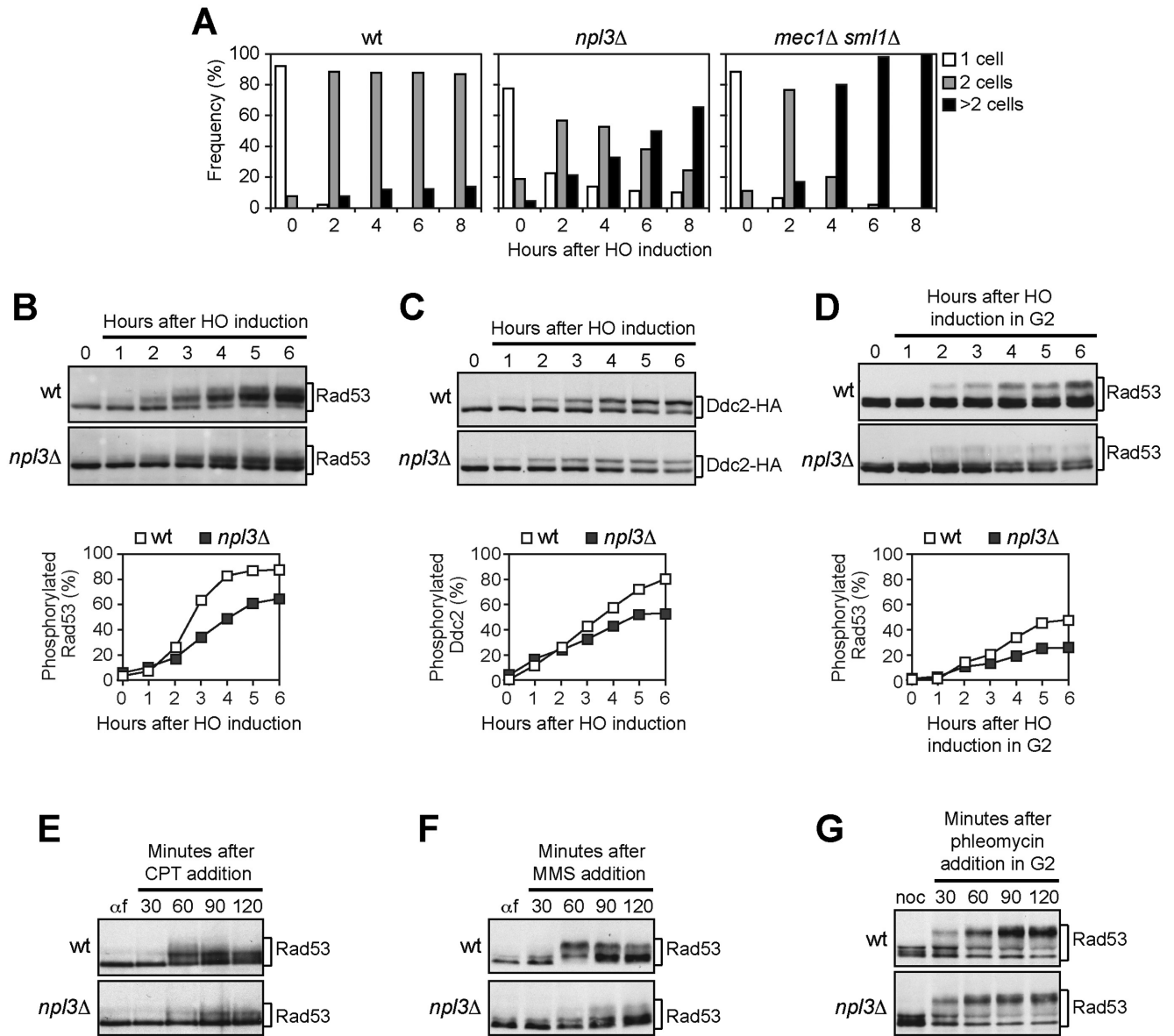
Figure 1. The lack of *NPL3* impairs Mec1 signaling activity. (**A**) YEPR G1-arrested cell cultures of JKM139 derivative strains were plated on galactose-containing plates to induce HO expression (time zero). At the indicated time points, 200 cells for each strain were analyzed to determine the frequency of unbudded cells, large budded cells and microcolonies with more than two cells. (**B** and **C**) Exponentially growing YEPR cell cultures expressing a fully functional Ddc2-HA protein were transferred to YEPRG (time zero). Protein extracts prepared at the indicated time points were subjected to western blot with anti-Rad53 (**B**) or anti-HA (**C**) antibodies. Quantitative analysis of Rad53 and Ddc2 phosphorylation was performed by calculating the ratio of band intensities for slowly-migrating bands to total amount of protein, and dividing the obtained values by the HO cleavage efficiency. Cut efficiency was evaluated as the difference in the normalized amount of qPCR products obtained with a primer pair that amplifies only the uncut *MAT* locus before and 2 h after galactose addition. (**D**) YEPR G2-arrested cell cultures were transferred in YEPRG (time zero) in the presence of nocodazole. Protein extracts were analyzed by western blot with anti-Rad53 antibodies. Quantitative analysis of Rad53 phosphorylation was performed as in (**B**). (**E** and **F**) YEPD G1-arrested cell cultures were released in fresh medium containing camptothecin (CPT) (50 μM) (**E**) or methyl methanesulfonate (MMS) (0,02%) (**F**). Rad53 phosphorylation was monitored by western blot with anti-Rad53 antibodies. (**G**) Phleomycin (15 μg/ml) was added to YEPD G2-arrested cell cultures kept arrested in G2. Protein extracts were subjected to western blot with anti-Rad53 antibodies.

rylated forms to total protein amount, and normalizing this value with respect to the efficiency of DSB formation evaluated by qPCR. Slowly-migrating Rad53 bands appeared 2–3 hours after HO induction and then became prevalent in wild type extracts (Figure 1B). Conversely, the unphosphorylated Rad53 species remained abundant until the end of the experiment in *npl3Δ* extracts although some slowly-migrating bands appeared 3–4 hours after HO induction (Figure 1B), indicating that Npl3 promotes the HO-induced Rad53 phosphorylation. Npl3 enhances also the phosphorylation of the Mec1-specific target Ddc2, as the amount of phosphorylated Ddc2 was lower in *npl3Δ* extracts than in wild type after HO induction (Figure 1C). Altogether, these results indicate that Npl3 promotes the activation of the Mec1-dependent checkpoint in response to a single irreparable DSB.

As cells lacking Npl3 showed growth defects (20), we asked whether their checkpoint defect could be ascribed to alterations in cell cycle progression. This was not the case, because Rad53 phosphorylation was defective in *npl3Δ* cells even when the HO cut was induced in cells arrested in G2 with nocodazole and kept in G2 throughout the experiment (Figure 1D).

To test whether Npl3 participates to checkpoint activation specifically after a single HO-induced DSB, we analyzed Rad53 phosphorylation in wild type and *npl3Δ* cells treated with different genotoxic agents. Cell cultures were arrested in G1 with α-factor and released in the presence of the topoisomerase poison camptothecin (CPT) or the alkylating agent MMS. As expected (38), Rad53 phosphorylation was slightly induced by CPT in wild type cells (Figure 1E). However, this phosphorylation was further reduced in *npl3Δ* cells (Figure 1E). Similarly, Rad53 was less phosphorylated in MMS-treated *npl3Δ* cells than in wild type (Figure 1F). Conversely, Rad53 was efficiently phosphorylated in both wild type and *npl3Δ* cells arrested in G2 and treated with the DSB-inducing drug phleomycin (Figure 1G). As checkpoint activation in all these conditions depends specifically on Mec1 (38,39), these results suggest that Npl3 is not directly required to activate Mec1 but rather to generate specific signals that activate Mec1.

Npl3 promotes the generation of ssDNA at DSBs

Mec1 activation requires the formation of RPA-coated ssDNA, which is generated by the 5′-3′ nucleolytic degradation of the DSB ends (10). In both *Schizosaccharomyces pombe* and human cells, RPA loading at DSB ends was found to be inhibited by the presence of DNA:RNA hybrids (40,41). As Npl3 counteracts the accumulation of DNA:RNA hybrids during transcription (20), the reduced Mec1 activation in *npl3Δ* cells could be due to the inability of these cells to remove DNA:RNA hybrids from the DSB ends. If this were the case, the checkpoint defect of *npl3Δ* cells should be alleviated by high levels of ribonuclease H1 (RNase H1), which is known to remove DNA:RNA hybrids *in vivo* (27). We therefore transformed wild type and *npl3Δ* cells carrying the HO system with a centromeric plasmid carrying the RNase H1-encoding gene (*RNH1*) under the control of *tetO* promoter, which acts as a strong promoter in the absence of tetracyclin (27). As expected

(20), the *tetO-RNH1* plasmid suppressed the hypersensitivity of *npl3Δ* cells spotted on plates with MMS (Figure 2A). However, the hypersensitivity to CPT of the same cells was only very slightly suppressed by RNase H1 overproduction (Figure 2A), which was also unable to restore the HO-induced checkpoint in cells lacking Npl3. In fact, *npl3Δ* cells carrying either the *tetO-RNH1* plasmid or the empty vector showed similar defects in both Rad53 phosphorylation (Figure 2B) and cell cycle arrest after HO induction compared to wild type cells (Supplementary Figure S2). This finding indicates that the checkpoint defect of *npl3Δ* cells is not likely due to DNA:RNA hybrid accumulation.

We then asked whether Npl3 promotes DSB processing by directly monitoring ssDNA generation at the DSB ends. Galactose was added to cell cultures arrested in G2 with nocodazole to produce the HO-induced DSB in cells that were then maintained in G2. Because ssDNA is resistant to cleavage by restriction enzymes, we measured the 5′ strand degradation of one DSB end by following the loss of SspI restriction fragments at different time points after galactose addition by Southern blot of genomic DNA under alkaline conditions, using a single-stranded RNA probe that anneals to the unresected 3′ strand on one side of the break (Figure 2C and D). We then evaluated the resection efficiency by calculating the ratio of band intensities for ssDNA to total amount of DNA, normalized with respect to the efficiency of DSB formation for each time point (Figure 2E). The 1.7 and 3.5 kb resection fragments (r1-r2 in Figure 2C–E) appeared with similar kinetics in both wild type and *npl3Δ* cells, suggesting that the lack of Npl3 does not affect initiation of DSB resection. However, the generation of resection fragments longer than 3.5 kb (r3–r7 in Figure 2C–E) was severely affected by the absence of Npl3 (Figure 2D and E), indicating that *npl3Δ* cells are specifically impaired in extensive resection. Thus, Npl3 is dispensable to initiate DSB resection, whereas it is required to produce long ssDNA tails.

The Npl3 RNA-binding domains are required for Npl3 functions in the DDR

Npl3 binds RNA through the RNA recognition motifs RRM1 and RRM2 (17). We therefore investigated whether the integrity of Npl3 RRMs is required for cell survival in the presence of DNA damage and/or HO-induced checkpoint activation. We transformed *npl3Δ* cells with either an empty centromeric plasmid or with similar plasmids carrying wild type *NPL3*, the *npl3-F160L* allele, which inactivates RRM1, the *npl3-SNK* (*L225S, G241N, E244K*) allele, which inactivates RRM2, and the *npl3-LSNK* (*F160L, L225S, G241N, E244K*) allele, which disrupts both RRM domains (17,29). Cells expressing the *npl3-F160L* allele were as sensitive as wild type to CPT (Figure 3A) and phosphorylated Rad53 similarly to wild type cells after HO-induction (Figure 3B and Supplementary Figure S3). By contrast, *npl3-SNK* and *npl3-LSNK* cells were more sensitive than wild type to CPT, although their hypersensitivity was less pronounced compared to *npl3Δ* cells (Figure 3A). Furthermore, the HO-induced Rad53 phosphorylation was reduced in *npl3-SNK* and *npl3-LSNK* mutants, similar to *npl3Δ* cells (Figure 3B).
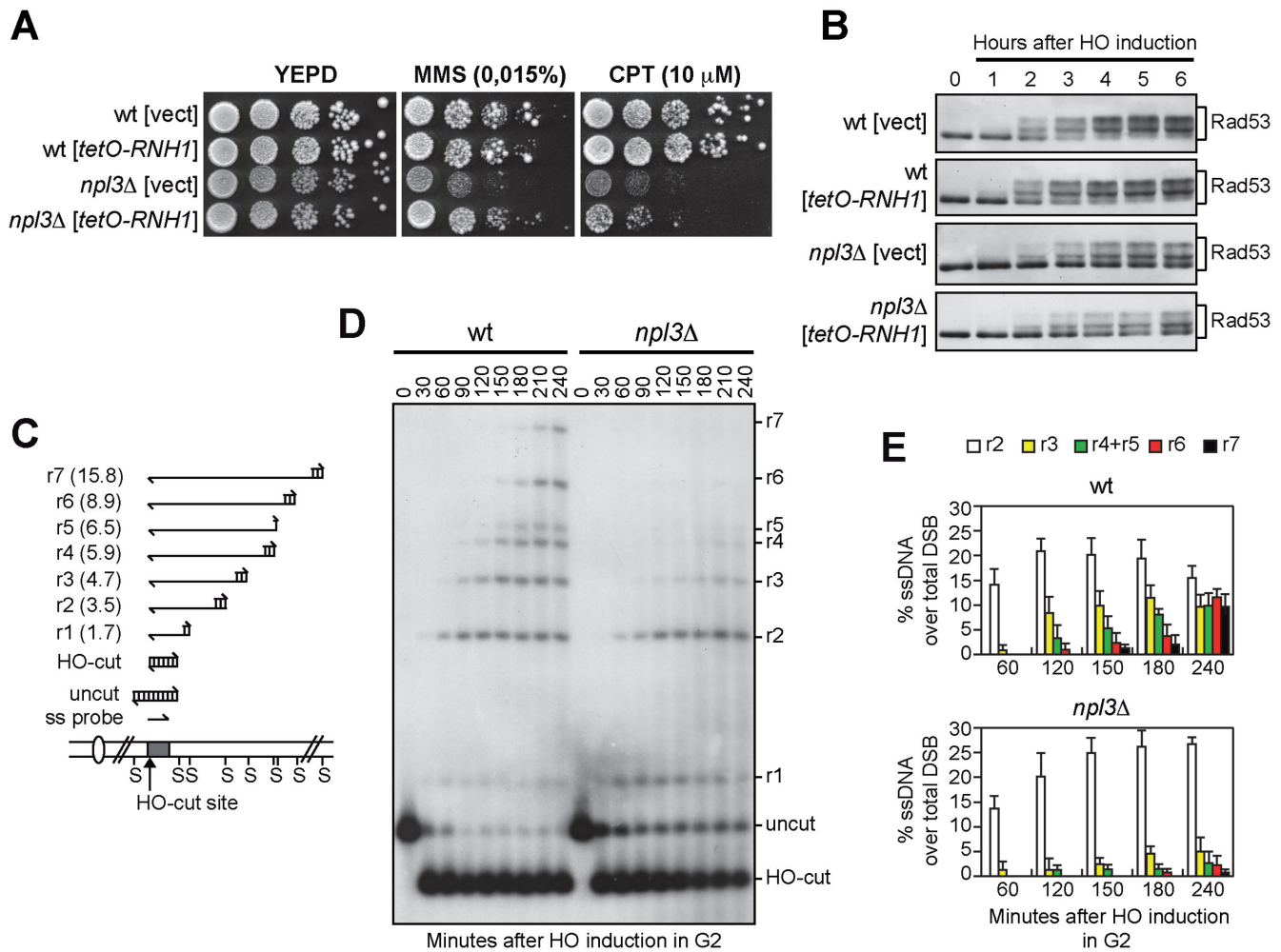
Figure 2. The lack of *NPL3* impairs extensive resection of DSB ends. (**A** and **B**) Exponentially growing cell cultures of wild type and *npl3Δ* strains, both carrying a centromeric plasmid either expressing the *RNH1* gene from the *tetO* promoter or empty (vect), were either serially diluted (1:10) before being spotted out onto YEPD plates with or without MMS or CPT (A), or transferred to YEPRG to monitor Rad53 phosphorylation by western blot (B). (**C**) System to detect DSB resection. Gel blots of SspI-digested genomic DNA separated on alkaline agarose gel were hybridized with a single-stranded RNA *MAT* probe (ss probe) that anneals to the unresected strand. 5′-3′ resection progressively eliminates SspI sites (S), producing larger SspI fragments (r1 through r7) detected by the probe. (**D** and **E**) Exponentially growing YEPR cell cultures were arrested in G2 with nocodazole and transferred to YEPRG (time zero) in the presence of nocodazole. (D) DSB resection as described in (C). (E) Resection products in (D) were analyzed by densitometry. The mean values are represented with error bars denoting SD (*n* = 5).

We also analyzed whether the integrity of Npl3 RRM domains is required for resection by measuring ssDNA generation at the HO-induced DSB in *npl3-LSNK* mutant cells. Similar to the absence of Npl3, the *npl3-LSNK* allele impairs long-range resection. In fact, the r3–r7 resection fragments accumulated less efficiently in both *npl3Δ* and *npl3-LSNK* cells than in wild type (Figure 3C and D). These results indicate that the RRM domains are required to support Npl3 functions in the DDR, with RRM2 playing a major role, suggesting that Npl3 regulates specific RNA molecules involved in the DDR.

The lack of Npl3 reduces Exo1 levels

Npl3 might either directly participate in resection or support DSB processing by promoting the expression of resection proteins. To discriminate between these two possibilities, we first evaluated whether Npl3 is recruited to

DNA ends. Chromatin immunoprecipitation (ChIP) and real-time qPCR were performed after generation of an HO-induced DSB in G2-arrested cells expressing a fully functional Npl3-HA variant. Similar amounts of DNA at 0.6 or 5.4 kb from the HO-cut site were recovered in immunoprecipitates from cells expressing either the Npl3-HA variant or untagged Npl3 both before and after DSB formation (Supplementary Figure S4). This suggests that Npl3 is not bound/recruited to DSB ends and thus does not directly participate in resection.

Generation of ssDNA at DSBs is promoted by several proteins, which control either initiation (Mre11, Rad50, Xrs2 and Sae2) or extension (Dna2, Sgs1 and Exo1) of resection (3,4). To assess whether Npl3 supports DSB processing by promoting the expression of resection factors, we measured the amount of the above proteins by western blot of protein extracts from wild type and *npl3Δ* cells ex-
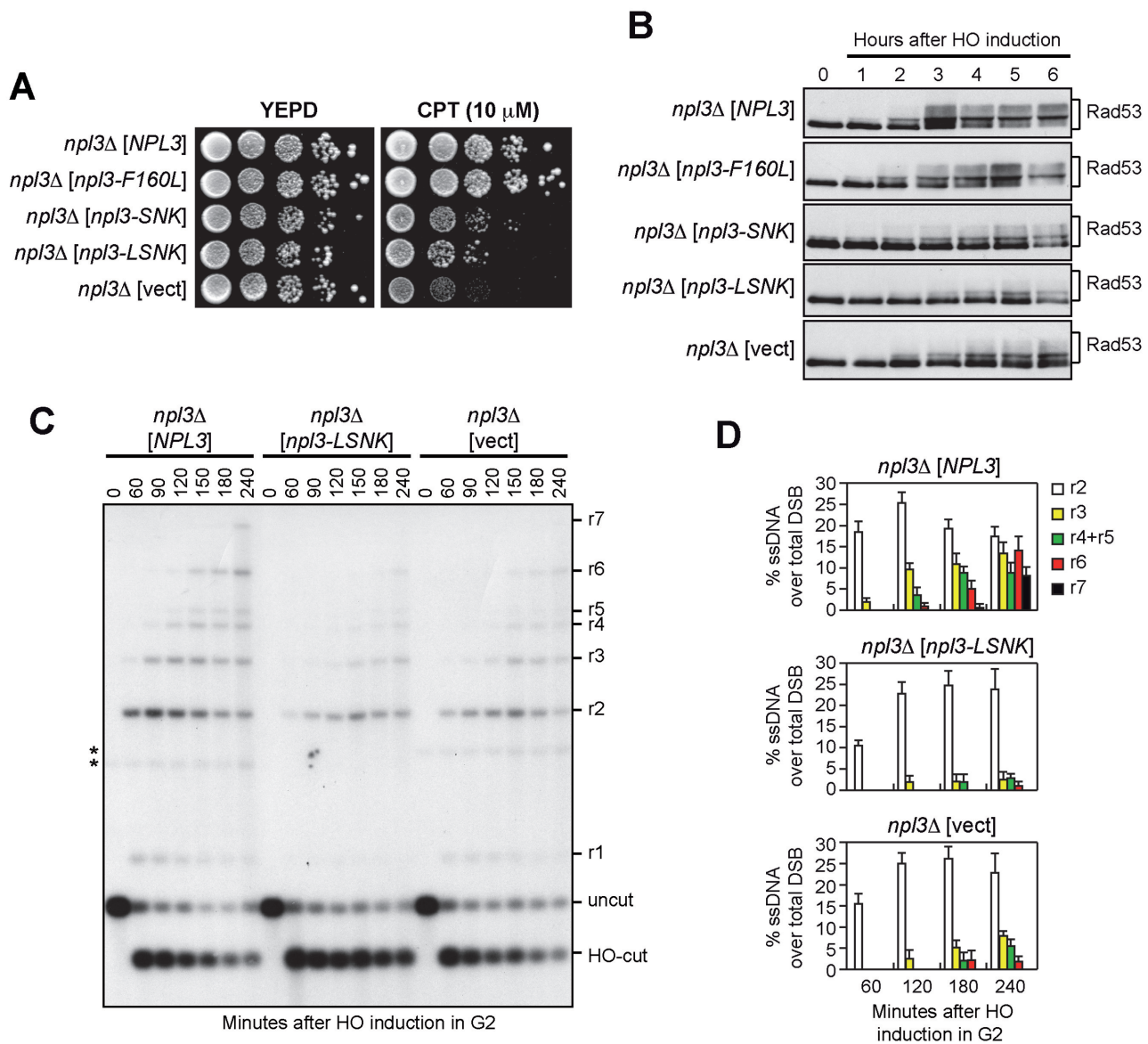
Figure 3. The Npl3 RNA binding domains are required for checkpoint and resection. (**A–D**) Exponentially growing cell cultures of a *npl3Δ* strain transformed with an empty centromeric vector (vect) or with the same vector carrying either the wild type *NPL3* gene or the indicated *npl3* mutant alleles were either spotted out onto YEPD plates with or without CPT (A), or transferred to YEPRG to follow Rad53 phosphorylation by western blot (B), or arrested in G2 and transferred to YEPRG (time zero) in the presence of nocodazole to monitor DSB resection as described in Figure 2C (C). *indicates cross hybridization signals likely due to the presence of the plasmids. (D) Resection products in (C) were analyzed by densitometry. The mean values are represented with error bars denoting SD (*n* = 3).

pressing fully functional tagged versions of these proteins and treated with galactose to induce the HO cut. Similar amounts of Sgs1 (Figure 4A), Mre11 and Xrs2 (Supplementary Figure S5A and B) were detected in wild type and *npl3Δ* cells, indicating that Npl3 does not control the levels of these proteins. Consistent with the checkpoint defect of *npl3Δ* cells, Xrs2 and Sgs1, which are known to undergo DNA damage-induced phosphorylation (39,42), were less phosphorylated in *npl3Δ* cells compared to wild type (Figure 4A and Supplementary Figure S5B). The amount of Dna2 (Figure 4B), Rad50 and Sae2 (Supplementary Figure S5C and D) was higher in *npl3Δ* cells than in wild type. However, it is unlikely that these effects can account for

the resection defect of *npl3Δ* cells. In fact, overexpression of neither *SAE2* nor *DNA2* affects ssDNA generation at DSB ends in wild type cells (43,44). Furthermore, Rad50 forms the MRX complex together with Mre11 and Xrs2, and Mre11 was found to be limiting for the recruitment of the MRX complex to DSBs (45), suggesting that high Rad50 levels should not affect DSB resection because they do not increase MRX recruitment to DSBs.

Interestingly, the amount of Exo1 was strongly reduced in *npl3Δ* cells compared to wild type both in raffinose and after galactose addition (Figure 4C). As Exo1 levels were not affected by treatment with the proteasome inhibitor MG132 of either wild type or *npl3Δ* cells exponentially
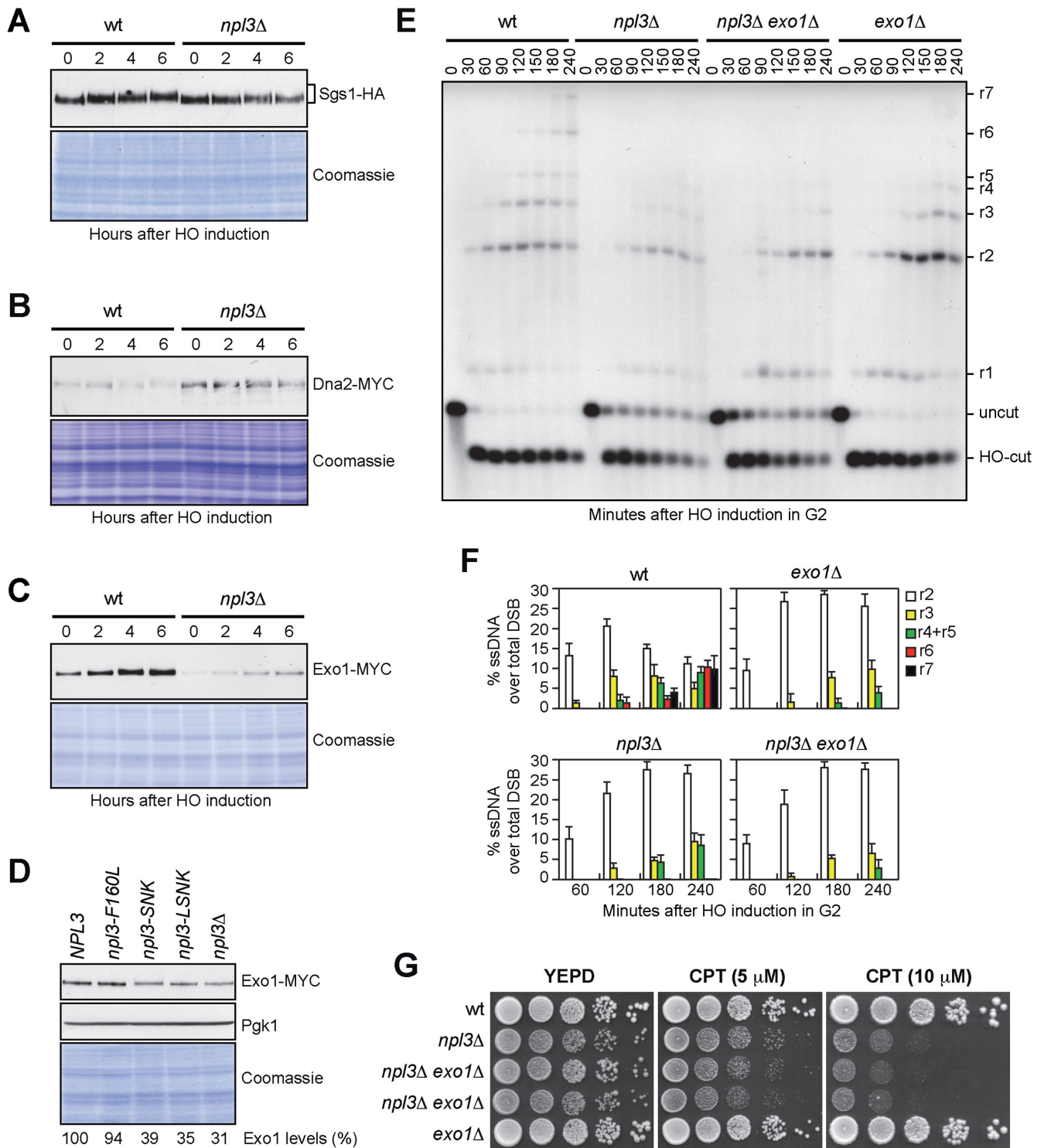
Figure 4. *NPL3* and *EXO1* belong to the same resection pathway. (**A–C**) Exponentially growing YEPR cell cultures of strains expressing the indicated tagged proteins were transferred to YEPRG (time zero). The same amounts of protein extracts were separated on SDS-PAGE and either subjected to western blot with antibodies specific for the indicated tags or stained with Coomassie as a loading control. (**D**) The same amounts of protein extracts prepared from exponentially growing YEPD cultures of strains as in Figure 3, all expressing the Exo1-MYC tagged protein, were either stained with Coomassie or subjected to western blot with anti-MYC and anti-Pgk1 (loading control) antibodies. The relative intensity of the Exo1-MYC signal compared to wild type (set to 100%) was estimated after normalization to the Pgk1 band. (**E** and **F**) G2-arrested cell cultures of the indicated strains were transferred to YEPRG (time zero) in the presence of nocodazole. (E) DSB resection as described in Figure 2C. (F) Resection products in (E) were analyzed by densitometry. The mean values are represented with error bars denoting SD (*n* = 3). (**G**) Exponentially growing cell cultures of the indicated strains were spotted out onto YEPD plates with or without CPT.

growing in glucose (Supplementary Figure S6), altogether these data indicate that Npl3 promotes Exo1 production independently of both the DNA damage and the carbon source.

We investigated whether the integrity of the Npl3 RRM motifs is important to regulate Exo1 levels by evaluating the amount of MYC-tagged Exo1 in cells expressing RRM1 and/or RRM2 defective Npl3 variants. The amount of Exo1, quantified using Pgk1 as a normalization control, was reduced of ∼70% in YEPD exponentially growing *npl3Δ* cells compared to wild type (Figure 4D). Npl3 interaction with RNA is important to regulate Exo1 levels, as we detected a similar reduction in *npl3-LSNK* and *npl3-SNK* mutant cells, although inactivation of only RRM1 did not affect Exo1 amount (Figure 4D).

NPL3 and *EXO1* belong to the same epistasis group for resection

As Exo1 is required for extensive resection of DNA ends (46,47), the low Exo1 levels in *npl3Δ* cells could be the cause of the resection defect of these cells. If this were the case, *npl3Δ* and *exo1Δ* cells should show a similar resection defect, and the lack of Exo1 should not increase the resection defect of *npl3Δ* cells. When we monitored ssDNA generation at the HO-induced DSB, both *exo1Δ* and *npl3Δ* single mutant cells efficiently initiated resection, but were impaired in the generation of the r3-r7 ssDNA products, and a similar defect in long-range resection was detectable in *npl3Δ exo1Δ* double mutant cells (Figure 4E). Although the HO-cut is induced more efficiently in *exo1Δ* cells (98%) than in both *npl3Δ* and *npl3Δ exo1Δ* cells (83% and 79%, respectively), a quantitative analysis of the resection products normalized to the cleavage efficiency confirmed that the resection kinetics were similar in these three mutant strains (Figure 4F).

The lack of Exo1 exacerbates the hypersensitivity to DNA damaging agents of mutants affecting other resection pathways, such as *sae2Δ* or *sgs1Δ* (47,48). Similarly, *NPL3* deletion increased the hypersensitivity to CPT of *sae2Δ* cells (Supplementary Figure S7A). Furthermore, the *npl3Δ sgs1Δ* spores obtained by tetrad dissection of a sporulated *NPL3/npl3Δ SGS1/sgs1Δ* diploid strain generated very small colonies (Supplementary Figure S7B), suggesting that Npl3 and Sgs1 participate in different pathways to support cell viability. Conversely, *EXO1* deletion neither increased the growth defect nor the hypersensitivity to CPT of *npl3Δ* cells (Figure 4G), indicating that Exo1 and Npl3 belong to the same resection pathway.

Exo1 high levels partially restore resection in *npl3Δ* cells

If the low Exo1 amount causes the resection defect in *npl3Δ* cells, increased Exo1 levels are expected to restore resection in these cells. We therefore monitored the resection kinetics in wild type and *npl3Δ* cells carrying a high copy number 2μ plasmid with the *EXO1* gene (28). The *EXO1* 2μ plasmid markedly increased the amount of long resection products in *npl3Δ* cells compared to the empty vector (Figure 5A and B). In particular, *npl3Δ* cells with the empty vector were specifically impaired in the generation of resection

fragments longer then 3.5 kb, while these longer ssDNA fragments appeared in *npl3Δ* cells carrying the *EXO1* 2μ plasmid. This indicates that Npl3 promotes the generation of long ssDNA tails by positively regulating Exo1 levels.

To verify that the *EXO1* 2μ plasmid increased Exo1 amount in the absence of Npl3, a 2μ plasmid either empty or carrying the *EXO1-MYC* allele was transformed into wild type and *npl3Δ* cells expressing the Exo1-Myc variant from the *EXO1* genomic locus. Although the Exo1 levels were increased by the *EXO1-MYC* 2μ plasmid in both wild type and *npl3Δ* cells, some fast-migrating Exo1 forms appeared specifically in *npl3Δ* cells (Figure 5C), suggesting that overproduced Exo1 may be unstable in the absence of Npl3. This might explain why the *EXO1-MYC* 2μ plasmid only partially restores resection in *npl3Δ* cells (Figure 5A and B).

Interestingly, the *EXO1* 2μ plasmid partially suppressed the hypersensitivity to CPT of *npl3Δ* cells (Figure 5D), indicating that the hypersensitivity of cells lacking Npl3 is at least partially due to the resection defect. Conversely, this plasmid did not suppress the hypersensitivity to MMS of *npl3Δ* cells (Figure 5D), nor the elevated levels of spontaneous recombination caused by the Npl3 lack (Supplementary Figure S8). To measure mitotic recombination frequency, we used strains carrying the *his3-513::TRP1::his3-537* heteroallelic duplication on chromosome XV (49) and transformed with either the *EXO1* 2μ plasmid or the empty vector. As expected (20), *NPL3* deletion increased 12.8-fold the recombination frequency at the *HIS3* locus compared to wild type cells (Supplementary Figure S8). The *EXO1* 2μ plasmid did not reduce, but rather slightly increased the recombination frequency in both wild type and *npl3Δ* cells (Supplementary Figure S8), indicating that the high recombination frequency in *npl3Δ* cells is not due to the low amount of Exo1.

The *EXO1* 2μ plasmid was also unable to restore the DSB-induced checkpoint in *npl3Δ* cells. In fact, HO-induced *npl3Δ* cells carrying either the empty vector or the *EXO1* 2μ plasmid showed similar defective Rad53 phosphorylation compared to wild type cells (Figure 5E and Supplementary Figure S9), indicating that the checkpoint defect of *npl3Δ* cells cannot be ascribed only to the resection defect. This result, together with the finding that the lack of Exo1 only very slightly affects the HO-induced Rad53 phosphorylation despite the resection defect (35,50), suggests that Npl3 might control the levels of other checkpoint proteins. However, we detected similar amounts of the three RPA subunits Rfa1, Rfa2 and Rfa3 in wild type and *npl3Δ* cells (Supplementary Figure S10A–C). Furthermore, the abundance of the checkpoint proteins Tel1, Ddc2, Rad53, and Rad9 was unaffected by the absence of Npl3 (Supplementary Figure S10D-F). Conversely, the amount of Mec1 was slightly lower in *npl3Δ* cells than in wild type (Supplementary Figure S10E). However, a Mec1-dependent checkpoint is strongly activated in *npl3Δ* cells treated with phleomycin (Figure 1G), suggesting that the slightly reduced amount of Mec1 detected in *npl3Δ* cells does not likely account for the checkpoint defect of the same cells. Altogether these results indicate that Npl3 plays two functions in the DDR: it promotes DSB resection by regu-
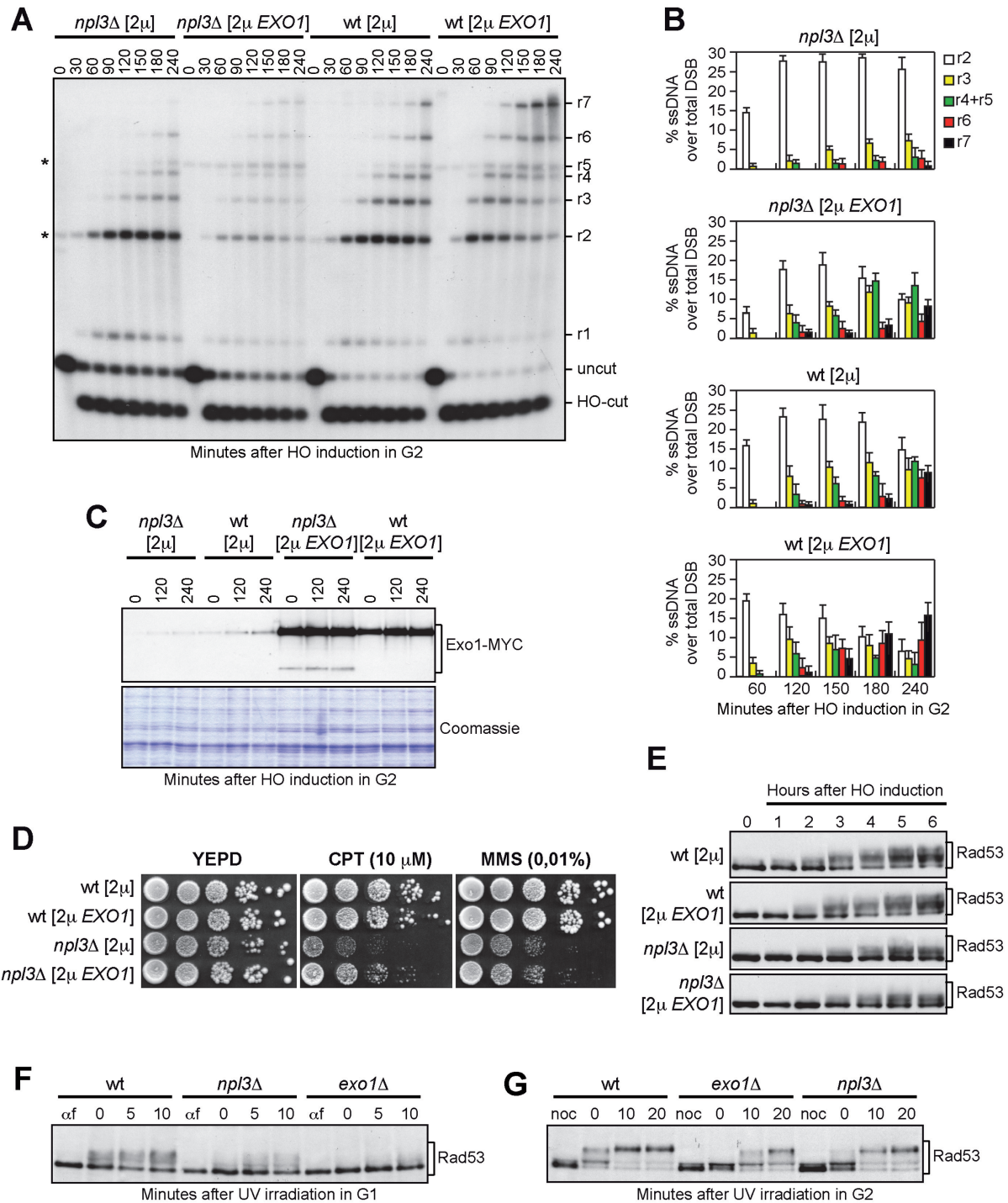
Figure 5. *EXO1* overexpression partially suppresses both the resection defect and the hypersensitivity to CPT of *npl3Δ* cells. (**A** and **B**) G2-arrested YEPR cell cultures of wild type and *npl3Δ* strains, both transformed with a 2µ plasmid either carrying the *EXO1* gene or empty (2µ), were transferred to YEPRG (time zero) in the presence of nocodazole. (A) DSB resection as described in Figure 2C. *indicates cross hybridization signals that partially overlap the r2 or r5 bands, and are due to the presence of the 2µ plasmid. (B) Resection products in (A) were analyzed by densitometry. The mean values are represented with error bars denoting SD (*n* = 3). (**C**) G2-arrested cell cultures of wild type and *npl3Δ* strains, both expressing the Exo1-MYC tagged protein from the *EXO1* locus and transformed with a 2µ plasmid either carrying the *EXO1-MYC* gene or empty (2µ), were transferred to YEPRG (time zero) in the presence of nocodazole. The same amounts of protein extracts were either subjected to western blot with anti-MYC antibodies or stained with Coomassie as a loading control. (**D** and **E**) Exponentially growing cell cultures of the strains described in (A and B) were either spotted out onto YEPD plates with or without CPT or MMS (D), or transferred to YEPRG (time zero) to analyze Rad53 phosphorylation by western blot with anti-Rad53 antibodies (E). (**F**) YEPD G1-arrested cell cultures (αf) of the indicated strains were UV irradiated (75 J/m^2) (time zero) and held in G1 in the presence of α-factor. Protein extracts were subjected to western blot with anti-Rad53 antibodies. (**G**) YEPD G2-arrested cell cultures (noc) of the strains in (F) were UV irradiated (75 J/m^2) (time zero) and held in G2 in the presence of nocodazole. Protein extracts were analyzed by western blot with anti-Rad53 antibodies.

lating Exo1 levels and it contributes to checkpoint activation by regulating some still unknown targets.

Npl3 and Exo1 are required for checkpoint activation after UV irradiation

If the Npl3-mediated control of Exo1 protein levels is biologically relevant, we expect *exo1Δ* and *npl3Δ* cells to show some common phenotypes. Exo1 is required to activate the checkpoint after UV treatment in non-cycling cells by promoting the generation of large ssDNA gaps during nucleotide excision repair (NER) processing (51). We then asked whether *npl3Δ* cells fail to activate the UV-induced checkpoint in G1- and G2-arrested cells, similarly to *exo1Δ* cells. Wild type, *npl3Δ* and *exo1Δ* cells were arrested either in G1 with α-factor or in G2 with nocodazole, UV irradiated, and transferred in fresh medium containing α-factor or nocodazole, respectively, to maintain the cell cycle arrests, as confirmed by FACS analyses (Supplementary Figure S11). As expected (51), Rad53 hyperphosphorylated forms appeared immediately after UV irradiation in wild type cells arrested either in G1 (Figure 5F) or in G2 (Figure 5G), while they were strongly reduced in similarly treated *exo1Δ* cells (Figure 5F and G). Also the lack of Npl3 impaired Rad53 phosphorylation in both G1 (Figure 5F) and G2 (Figure 5G), although to a lesser extent than the absence of Exo1 (Figure 5F and G), possibly because Exo1 is not totally absent in *npl3Δ* cells (Figure 4C and D). Thus, similarly to Exo1, Npl3 is required for checkpoint activation after UV irradiation in G1 and in G2. As Npl3 is not required *per se* to activate the checkpoint, at least in G2-arrested cells (Figure 1G), these results suggest that the low Exo1 levels in *npl3Δ* cells are not sufficient to efficiently process the UV lesions and generate enough ssDNA to activate the checkpoint in non-cycling cells.

Abnormal *EXO1* RNA species are produced in the absence of Npl3

Genome-wide analyses have shown that the absence of Npl3 results in either down- or up-regulation of many protein-coding genes (20,23,52). These analyses did not show significant differences in *EXO1* expression in *npl3Δ* versus wild type cells, suggesting that Npl3 controls the abundance of the Exo1 protein by acting at post-transcriptional level. To verify this possibility, we first employed quantitative reverse transcriptase PCR (qRT-PCR) to measure the amount of *EXO1* RNA either in the presence or in the absence of Npl3. Total RNA was extracted from wild type, *npl3Δ* and *exo1Δ* cells exponentially growing in YEPD and subjected to reverse transcription followed by quantitative real-time PCR with primer pairs located either inside the *EXO1* coding region (PP1 in Figure 6A) or the *ALG9* control gene. The amount of *EXO1* RNA was not diminished in the absence of Npl3 (Figure 6B). Rather, we found a modest increase of *EXO1* RNA levels in *npl3Δ* cells compared to wild type (Figure 6B). The levels of the Exo1 protein (Figure 4C and D) were monitored by using a tagged version of the protein generated by inserting a 18 MYC epitopes coding sequence just before the *EXO1* stop codon. Similarly to *EXO1* RNA, the *EXO1-MYC* RNA was slightly more abundant in *npl3Δ*

cells than in wild type (Figure 6B), indicating that neither Npl3 nor the insertion of the MYC coding sequence into the *EXO1* gene affects *EXO1* transcription.

If Npl3 promoted *EXO1* pre-mRNA processing, *npl3Δ* cells should accumulate aberrant RNA molecules. Thus, the same RNA extracts were analyzed by northern blot with a 1437 nt DNA probe complementary to the *EXO1* coding sequence (Figure 6A). The probe was specific for the *EXO1* RNA species, as no signal was detected in RNA prepared from *exo1Δ* cells (Figure 6C). In wild type RNA extracts this probe revealed a single band that migrated between the two ribosomal RNA (rRNA) species 25S (3392 nt) and 18S (1798 nt), as expected for the *EXO1* RNA, whose length should be approximately 2400 nt, considering that the average *S. cerevisiae* mRNA consists of the protein coding sequence (2109 nt for *EXO1*) plus 260 nt of 5′ and 3′ untranslated sequences (53). The same probe detected at least 3 additional longer bands in the *npl3Δ* RNA preparation (Figure 6C), indicating that the absence of Npl3 leads to the generation of longer than normal *EXO1* RNA molecules. Similarly, a single *EXO1* RNA species migrating just below the 3392 nt-long 25S rRNA was detected in cells carrying the *EXO1-MYC* construct, while at least an additional longer band was present in RNA extracts from *npl3Δ EXO1-MYC* cells (Figure 6D). Furthermore, longer than normal *EXO1* RNA molecules were produced also in *npl3-LSNK* cells, where both Npl3 RRM domains were inactivated (Figure 6E). Thus, extended *EXO1* RNA species are produced in the absence of Npl3 or of its RNA-binding capacity, suggesting that Npl3 might regulate initiation, termination or processing of the *EXO1* transcript.

In order to verify whether the abnormal *EXO1* transcripts in *npl3Δ* cells are extended at the 5′ end, we performed 5′ rapid amplification of cDNA ends (5′-RACE) on wild type and *npl3Δ* RNA extracts that were subjected to reverse transcription with an *EXO1* specific primer. A poly(A) tail was added to the resulting cDNA, which was then used as a template for two subsequent PCR reactions with primers annealing to the appended tail and to the *EXO1* coding sequence. A PCR with primers located at the 5′ tail and 248 bp downstream the *EXO1* initiation codon revealed a ∼400 bp abundant product and two weak smaller products in wild type extracts, while a single slightly bigger band was detected in *npl3Δ* (Figure 6F). Although this result suggests that Npl3 influences the use of different transcription start sites in *EXO1* promoter, the small difference in length at the 5′ of the *EXO1* transcripts does not likely account for the extended RNA species observed by northern blot in *npl3Δ* cells (Figure 6C and E).

We then evaluated whether these transcripts were extended at the 3′ end, as Npl3 was recently found to prevent transcriptional readthrough of both protein-coding and non-coding genes (23). We therefore performed qRT-PCR analyses with different primer pairs located either internally to the *EXO1* coding sequence (PP1 and PP2), or 100, 300, 850, 1000 bp (PP3–PP6, respectively) downstream to the stop codon (Figure 6A). The RNA levels estimated with the different primer pairs were normalized with respect to the RNA levels evaluated with the PP1 primer pair, which were set to 1.0 for each strain (Figure 6G). The RNA levels estimated with the primer pair located immediately be-
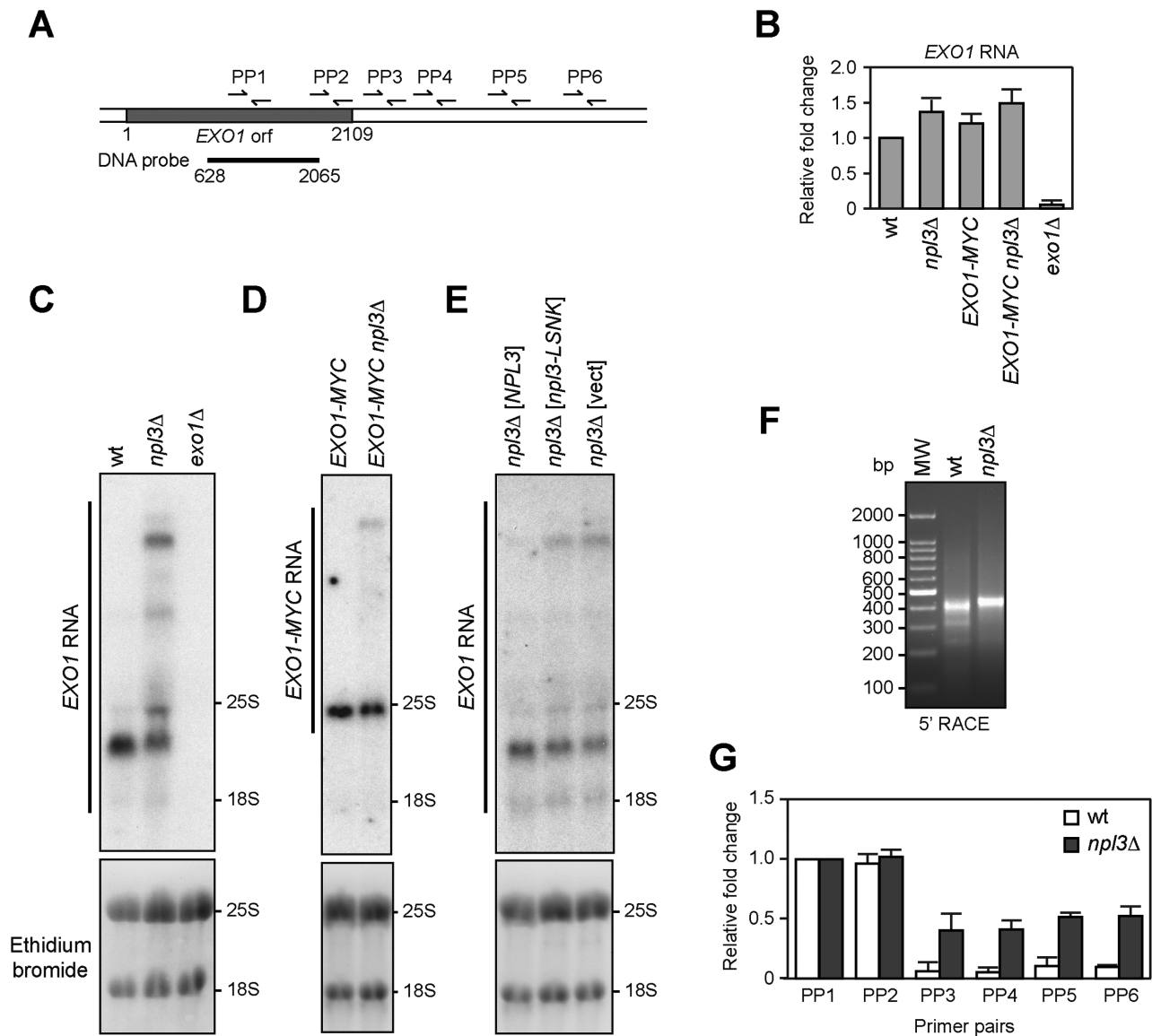
Figure 6. *EXO1* RNA in the absence of Npl3. (**A**) Schematic representation of the *EXO1* locus. Primer pairs (PP1-PP6) used for qRT-PCR are indicated by arrows. A bar indicates the 1437 bp-DNA probe internal to the *EXO1* coding sequence (+628 to + 2065 from the ATG initiation codon) used for northern blot. (**B**) Total RNA was extracted from exponentially growing YEPD cell cultures of the indicated strains and subjected to quantitative reverse transcriptase PCR (qRT-PCR) with primer pairs located into the *EXO1* (PP1 in (A)) and *ALG9* coding sequences. The *EXO1* RNA levels relative to wild type (set to 1.0) were calculated using $\Delta\Delta$Ct method after normalization to the *ALG9* RNA levels for each sample. The mean values are represented with error bars denoting SD ($n = 5$). (**C–E**) Total RNA extracted from the indicated cell cultures was subjected to northern blot and hybridized with the probe as in (A). The agarose gels were stained with ethidium bromide to detect 18S and 25S rRNAs (bottom). (**F**) Total RNA extracted from wild type and *npl3Δ* cells was subjected to 5′ RACE to visualize the *EXO1* 5′ partial cDNA ends. After reverse transcription with a *EXO1* specific primer and poly(A) tailing, two subsequent PCR reactions were performed with primers annealing to the appended tail and to the *EXO1* coding sequence 718 and 248 bp downstream the *EXO1* initiation codon. The final PCR products were separated on a 1.5% agarose gel and visualized with ethidium bromide. (**G**) Total RNA as in (F) was subjected to qRT-PCR with primer pairs depicted in (A), or located in the *ALG9* coding sequence. The amount of products obtained with different *EXO1* primer pairs was normalized to the *ALG9* product using $\Delta\Delta$Ct method. Then, the normalized RNA levels estimated with the different primer pairs in the *EXO1* locus were normalized to the RNA levels evaluated with the PP1 primer pair and set to 1.0 for each strain. The mean values are represented with error bars denoting SD ($n = 4$).

fore the stop codon (PP2) were almost identical to those evaluated with the primer pair internal to the *EXO1* coding sequence (PP1) in both wild type and *npl3Δ* extracts (Figure 6G). Strikingly, only *npl3Δ* extracts generated products with the primer pairs located downstream to the stop codon (PP3–PP6) (Figure 6G), although the amount of these products was lower (almost 40%) than that of the products obtained with primer pairs internal to the *EXO1* coding sequence (Figure 6G). These results indicate that a substantial fraction of *EXO1* RNA is not properly terminated in the absence of Npl3, thus generating RNA molecules with long 3′ tails that extend at least 1000 bp downstream to the *EXO1* stop codon.

Rrp6 controls the levels of the *EXO1* RNA

It is known that 3′-extended RNAs might be unstable and targeted to degradation by the RNA decay systems. In particular, defects in 3′-end processing result in nuclear retention and degradation of faulty transcripts mainly by the nuclear exosome (14). To test whether the nuclear exosome degrades the extended *EXO1* RNA molecules produced in the absence of Npl3, we checked if these abnormal *EXO1* RNAs further accumulate in *npl3Δ* cells lacking the exosome catalytic subunit Rrp6, whose lack was reported to impair viability of *npl3Δ* cells (54). In our genetic background, *npl3Δ rrp6Δ* spores generated by sporulation and tetrad dissection of a *NPL3/npl3Δ RRP6/rrp6Δ* diploid gave rise to very small colonies, which could be further propagated in YEPD, despite their growth defect (Figure 7A and E). We then subjected to both qRT-PCR and northern blot analysis the *EXO1* RNAs derived from exponentially growing wild type, *npl3Δ*, *rrp6Δ* and *npl3Δ rrp6Δ* cells. Both analyses revealed higher levels of *EXO1* RNA in *npl3Δ rrp6Δ* cells than in *npl3Δ* and *rrp6Δ* single mutants (Figure 7B and C). The intensity of the bands detected by the *EXO1* probe in the northern blot, and in particular that of the slowest migrating band, was higher in *npl3Δ rrp6Δ* RNA extracts than in *npl3Δ* (Figure 7C), suggesting that Rrp6 partially removes abnormal RNA intermediates that accumulate in the absence of Npl3.

As the amount of the 2400 nt-long *EXO1* RNA species was also higher in *npl3Δ rrp6Δ* cells compared to *npl3Δ* cells (Figure 7C), we asked whether the absence of Rrp6 also increased the levels of Exo1 protein in cells lacking Npl3. Indeed, the amount of the Exo1-MYC tagged variant was slightly higher in exponentially growing *npl3Δ rrp6Δ* cells than in *npl3Δ* cells (Figure 7D). This suggests that, in the presence of improperly processed transcripts, the exosome targets not only the faulty, but also some functional *EXO1* RNA molecules. Interestingly, although *npl3Δ rrp6Δ* cells grew poorly on YEPD plates (Figure 7A and E), they formed colonies in the presence of CPT more efficiently than *npl3Δ* cells (Figure 7E), similarly to what we observed with the overexpression of the *EXO1* gene (Figure 5D). Taken together, these results indicate that Npl3 promotes proper maturation of the *EXO1* RNA, thus preventing its degradation by the nuclear exosome.

DISCUSSION

Resection of DSB ends is a two-step process, which is initiated by MRX and Sae2 that induce an endonucleolytic cleavage of the 5′-terminated DNA strands. This cleavage promotes the access of the Exo1 and Dna2 nucleases, which allow the generation of long ssDNA tails (reviewed in (3,4)). Here, we show that the lack of the RBP Npl3 impairs the generation of long stretches of ssDNA at DSB ends and decreases the amount of the exonuclease Exo1. Furthermore, the lack of Exo1 does not exacerbate the resection defect of *npl3Δ* cells, while high Exo1 levels partially restore resection in these cells, indicating that Npl3 supports long-range resection by ensuring the production of a sufficient amount of Exo1.

We also found that Npl3 is required to activate a Mec1-dependent checkpoint in response to different kinds of DNA damage, but it is dispensable for checkpoint activation after phleomycin treatment in G2 (Figures 1 and 5). As Exo1 is required to generate long stretches of ssDNA (35,51,55), which are the signals that activate Mec1 at least in response to both DSBs and UV-induced DNA lesions (10,34,35,55,56), the reduced Exo1 amount in *npl3Δ* cells could account for the checkpoint defect of the same cells. However, *EXO1* overexpression does not alleviate the checkpoint defect of *npl3Δ* cells experiencing a single DSB. This result, together with the finding that the lack of Exo1 causes a very mild, if any, checkpoint defect in response to a single DSB (35,50), suggests that Npl3 regulates the functions of other proteins involved in checkpoint activation besides Exo1. Although genome-wide transcription analyses showed that most checkpoint genes are not significantly downregulated in the absence of Npl3 (20), a very mild decrease of *MEC1* gene expression was reported in *npl3Δ* cells (23), which also show a slight reduction in Mec1 protein abundance (Supplementary Figure S10E). Furthermore, *npl3Δ* cells show increased amounts of *SAE2* mRNA (23) that correlate with increased levels of the Sae2 protein (Supplementary Figure S5D). As high Sae2 levels have been shown to counteract Mec1-dependent checkpoint activation (50), the checkpoint defect of *npl3Δ* cells might be due to the high Sae2 levels. Thus, we speculate that the checkpoint defect of *npl3Δ* cells may result both from a defect in ssDNA generation due to low Exo1 levels and from a mild deregulation of factors involved in checkpoint signaling, such as Sae2 and Mec1. These Mec1 and Sae2 misregulations are likely not sufficient to impair checkpoint activation by themselves, as the checkpoint is strongly activated in *npl3Δ* cells treated with phleomycin. However, they might impair Mec1 recruitment/activation in response to DNA lesions that require extensive nucleolytic processing to be detected by Mec1, such as DSBs or UV-induced DNA lesions.

The idea that Npl3 regulates other DDR factors besides Exo1 is also supported by the observation that the lack of Npl3 causes hypersensitivity to DSB-inducing agents, whereas *EXO1* deletion does not (47,55). Accordingly, *EXO1* overexpression partially rescues the hypersensitivity to CPT of *npl3Δ* cells, while it does not affect the hypersensitivity of the same cells to MMS. This result also suggests that Exo1 is important to repair the damage induced by CPT, while other defects can contribute to the hy-
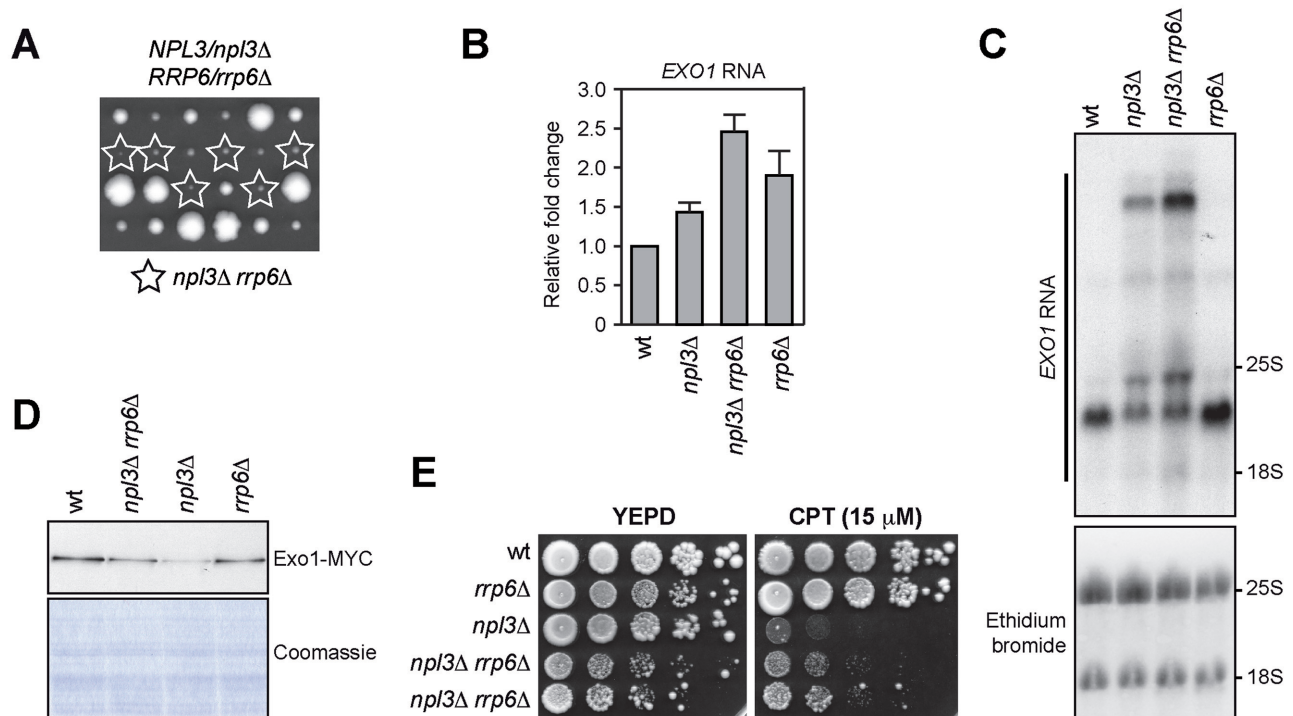
Figure 7. Rrp6 limits the accumulation of abnormal *EXO1* RNAs in the absence of Npl3. (**A**) Meiotic tetrads from diploid cells with the indicated genotype were dissected on YEPD plates that were incubated at 30°C for 3 days, followed by spore genotyping. (**B**, **C**) Total RNA was extracted from exponentially growing YEPD cultures of the indicated strains and subjected to both qRT-PCR as in Figure 6B and northern blot as in Figure 6C–E. (**D**) The same amounts of protein extracts prepared from exponentially growing cell cultures with the indicated genotypes and expressing the Exo1-MYC tagged protein were either stained with Coomassie or subjected to western blot with anti-MYC antibodies. (**E**) Exponentially growing cell cultures of the indicated strains were spotted out onto YEPD plates with or without CPT.

persensitivity to MMS of *npl3Δ* cells. One of these defects might be the replication stress caused by the accumulation of transcription-dependent DNA:RNA hybrids in the absence of Npl3. In fact, overproduction of RNaseH1, which removes these hybrids *in vivo* (20,27), suppresses the hypersensitivity to MMS (Figure 2A) and reduces the high levels of spontaneous mitotic recombination caused by the lack of Npl3 (20). On the contrary, *EXO1* overexpression does not reduce the recombination frequency in *npl3Δ* cells (Supplementary Figure S8).

How does Npl3 control the abundance of the Exo1 protein? As the low Exo1 amount in *npl3Δ* cells does not correlate with a decrease in total *EXO1* RNA levels (Figure 6) (20,23), we exclude that Npl3 promotes *EXO1* transcription. Rather, the extended *EXO1* RNA species detected in the absence of Npl3 may be due to termination defects and transcription readthrough. In fact, defects in transcription termination were seen for approximately 30% of protein-coding genes in *npl3Δ* cells (23), and we found that a region 1000 bp downstream to the *EXO1* stop codon was transcribed in *npl3Δ* cells but not in wild type, while we did not find a significant extension of the *EXO1* RNA 5' end in the absence of Npl3. Furthermore, Npl3 was found to be co-transcriptionally recruited to DNA at highly transcribed genes (among which *EXO1*), where it distributes in a gradient that increases toward the 3' end of the coding region (20), and to bind both the 5' (23,52) and the 3' ends of mRNAs (52). Npl3 inactivation is also known to impair mRNA

export and to cause the accumulation of transcripts in the nucleus (57). Taken together, these results suggest that, in the absence of Npl3, some *EXO1* nascent transcripts are not appropriately packaged, thus possibly interfering with the transcription termination process and forming abnormal *EXO1* RNA species that are not exported to the cytoplasm and/or not efficiently translated.

These abnormal *EXO1* RNAs are likely degraded, at least in part, by the nuclear exosome, as the lack of Rrp6 in *npl3Δ* cells results in a further accumulation of extended *EXO1* RNA species. Accordingly, the exosome was found to degrade transcripts that are not co-transcriptionally packaged because of mutations in the THO complex, which, similarly to Npl3, is required for pre-mRNA processing and export (58). The lack of Rrp6 slightly increases Exo1 protein levels in *npl3Δ* cells, suggesting that in the presence of faulty transcripts Rrp6 can sequester and/or degrade also functional RNAs. Rrp6 was found to prevent chromatin release of aberrant transcripts when co-transcriptional pre-mRNA processing fails, thus eventually providing these transcripts with additional time to complete their maturation (59,60). Furthermore, Rrp6 was recently reported to participate in mRNA nuclear retention caused by Npl3 inactivation. In fact, while *npl3* temperature-sensitive mutant cells accumulate mRNAs in the nucleus at the restrictive temperature, mRNAs are partially released in the cytoplasm in *npl3 rrp6* double mutant cells (61). Interestingly, Rrp6 deletion also partially suppresses the temperature sensitivity of these *npl3*

mutant cells, suggesting that part of the improperly packaged mRNAs produced in the absence of Npl3 may be functional, although incompetent for export (61).

Exo1 is an evolutionarily conserved processive exonuclease that can degrade several kilobases of DNA (7,8) and is implicated in a variety of DNA metabolic processes including DNA repair as well as processing of both stalled replication forks and uncapped telomeres (2,5,62–64). Exo1 action is modulated by both positive and negative regulators, which control Exo1 access to DNA and limit excessive DNA degradation (3,4,6–8). Exo1 expression is also induced during yeast meiosis to promote meiotic DSB processing and crossing over (65). In mammals, splicing of *EXO1* transcripts is facilitated after DNA damage by a splicing complex that contains the DDR protein BRCA1 (66). The Npl3-mediated regulation of Exo1 amount that we show here represents another level of control of Exo1 activity that guarantees the availability of suitable amounts of Exo1 to respond to DNA damage and maintain genome integrity.

SUPPLEMENTARY DATA

Supplementary Data are available at NAR Online.

ACKNOWLEDGEMENTS

FUNDING

REFERENCES

1. Ciccia,A. and Elledge,S.J. (2010) The DNA damage response: making it safe to play with knives. *Mol. Cell*, **40**, 179–204.
2. Symington,L.S., Rothstein,R. and Lisby,M. (2014) Mechanisms and regulation of mitotic recombination in Saccharomyces cerevisiae. *Genetics*, **198**, 795–835.
3. Daley,J.M., Niu,H., Miller,A.S. and Sung,P. (2015) Biochemical mechanism of DSB end resection and its regulation. *DNA Repair (Amst.)*, **32**, 66–74.
4. Villa,M., Cassani,C., Gobbini,E., Bonetti,D. and Longhese,M.P. (2016) Coupling end resection with the checkpoint response at DNA double-strand breaks. *Cell. Mol. Life Sci.*, **73**, 3655–3663.
5. Ferrari,M., Dibitetto,D., De Gregorio,G., Eapen,V.V., Rawal,C.C., Lazzaro,F., Tsabar,M., Marini,F., Haber,J.E. and Pellicioli,A. (2015) Functional interplay between the 53BP1-ortholog Rad9 and the Mre11 complex regulates resection, end-tethering and repair of a double-strand break. *PLoS Genet.*, **11**, e1004928.
6. Morin,I., Ngo,H.P., Greenall,A., Zubko,M.K., Morrice,N. and Lydall,D. (2008) Checkpoint-dependent phosphorylation of Exo1 modulates the DNA damage response. *EMBO J.*, **27**, 2400–2410.
7. Cannavo,E., Cejka,P. and Kowalczykowski,S.C. (2013) Relationship of DNA degradation by Saccharomyces cerevisiae Exonuclease 1 and its stimulation by RPA and Mre11-Rad50-Xrs2 to DNA end resection. *Proc. Natl. Acad. Sci. U.S.A.*, **110**, E1661–E1668.
8. Myler,L.R., Gallardo,I.F., Zhou,Y., Gong,F., Yang,S.H., Wold,M.S., Miller,K.M., Paull,T.T. and Finkelstein,I.J. (2016) Single-molecule imaging reveals the mechanism of Exo1 regulation by single-stranded DNA binding proteins. *Proc. Natl. Acad. Sci. U.S.A.*, **113**, E1170–E1179.
9. Nakada,D., Matsumoto,K. and Sugimoto,K. (2003) ATM-related Tel1 associates with double-strand breaks through an Xrs2-dependent mechanism. *Genes Dev.*, **17**, 1957–1962.
10. Zou,L. and Elledge,S.J. (2003) Sensing DNA damage through ATRIP recognition of RPA-ssDNA complexes. *Science*, **300**, 1542–1548.
11. Wickramasinghe,V.O. and Venkitaraman,A.R. (2016) RNA processing and genome stability: cause and consequence. *Mol. Cell*, **61**, 496–505.
12. Tutucci,E. and Stutz,F. (2011) Keeping mRNPs in check during assembly and nuclear export. *Nat. Rev. Mol. Cell Biol.*, **12**, 377–384.
13. Eberle,A.B. and Visa,N. (2014) Quality control of mRNP biogenesis: networking at the transcription site. *Semin. Cell Dev. Biol.*, **32**, 37–46.
14. Fox,M.J. and Mosley,A.L. (2016) Rrp6: Integrated roles in nuclear RNA metabolism and transcription termination. *Wiley Interdiscip. Rev. RNA*, **7**, 91–104.
15. García-Muse,T. and Aguilera,A. (2016) Transcription-replication conflicts: how they occur and how they are resolved. *Nat. Rev. Mol. Cell Biol.*, **17**, 553–563.
16. Janke,R., Kong,J., Braberg,H., Cantin,G., Yates,J.R., Krogan,N.J. and Heyer,W.D. (2016) Nonsense-mediated decay regulates key components of homologous recombination. *Nucleic Acids Res.*, **44**, 5218–5230.
17. Deka,P., Bucheli,M.E., Moore,C., Buratowski,S. and Varani,G. (2008) Structure of the yeast SR protein Npl3 and Interaction with mRNA 3′-end processing signals. *J. Mol. Biol.*, **375**, 136–150.
18. Dermody,J.L., Dreyfuss,J.M., Villén,J., Ogundipe,B., Gygi,S.P., Park,P.J., Ponticelli,A.S., Moore,C.L., Buratowski,S. and Bucheli,M.E. (2008) Unphosphorylated SR-like protein Npl3 stimulates RNA polymerase II elongation. *PLoS One*, **3**, e3273.
19. Lei,E.P., Krebber,H. and Silver,P.A. (2001) Messenger RNAs are recruited for nuclear export during transcription. *Genes Dev.*, **15**, 1771–1782.
20. Santos-Pereira,J.M., Herrero,A.B., García-Rubio,M.L., Marín,A., Moreno,S. and Aguilera,A. (2013) The Npl3 hnRNP prevents R-loop-mediated transcription-replication conflicts and genome instability. *Genes Dev.*, **27**, 2445–2458.
21. Bucheli,M.E., He,X., Kaplan,C.D., Moore,C.L. and Buratowski,S. (2007) Polyadenylation site choice in yeast is affected by competition between Npl3 and polyadenylation factor CFI. *RNA*, **13**, 1756–1764.
22. Wong,C.M., Tang,H.M., Kong,K.Y., Wong,G.W., Qiu,H., Jin,D.Y. and Hinnebusch,A.G. (2010) Yeast arginine methyltransferase Hmt1p regulates transcription elongation and termination by methylating Npl3p. *Nucleic Acids Res.*, **38**, 2217–2228.
23. Holmes,R.K., Tuck,A.C., Zhu,C., Dunn-Davies,H.R., Kudla,G., Clauder-Munster,S., Granneman,S., Steinmetz,L.M., Guthrie,C. and Tollervey,D. (2015) Loss of the yeast SR protein Npl3 alters gene expression due to transcription readthrough. *PLoS Genet.*, **11**, e1005735.
24. McKinney,J.S., Sethi,S., Tripp,J.D., Nguyen,T.N., Sanderson,B.A., Westmoreland,J.W., Resnick,M.A. and Lewis,L.K. (2013) A multistep genomic screen identifies new genes required for repair of DNA double-strand breaks in Saccharomyces cerevisiae. *BMC Genomics*, **14**, 251.
25. Pan,X., Ye,P., Yuan,D.S., Wang,X., Bader,J.S. and Boeke,J.D. (2006) A DNA integrity network in the yeast Saccharomyces cerevisiae. *Cell*, **124**, 1069–1081.
26. Smolka,M.B., Albuquerque,C.P., Chen,S.H. and Zhou,H. (2007) Proteome-wide identification of in vivo targets of DNA damage checkpoint kinases. *Proc. Natl. Acad. Sci. U.S.A.*, **104**, 10364–10369.
27. Castellano-Pozo,M., García-Muse,T. and Aguilera,A. (2012) R-loops cause replication impairment and genome instability during meiosis. *EMBO Rep.*, **13**, 923–929.
28. Sokolsky,T. and Alani,E. (2000) EXO1 and MSH6 are high-copy suppressors of conditional mutations in the MSH2 mismatch repair gene of Saccharomyces cerevisiae. *Genetics*, **155**, 589–599.

29. Lee-Soety,J.Y., Jones,J., MacGibeny,M.A., Remaly,E.C., Daniels,L., Ito,A., Jean,J., Radecki,H. and Spencer,S. (2012) Yeast hnRNP-related proteins contribute to the maintenance of telomeres. *Biochem. Biophys. Res. Commun.*, **426**, 12–17.

30. Trovesi,C., Falcettoni,M., Lucchini,G., Clerici,M. and Longhese,M.P. (2011) Distinct Cdk1 requirements during single-strand annealing, noncrossover, and crossover recombination. *PLoS Genet.*, **7**, e1002263.

31. Gietz,R.D. and Sugino,A. (1988) New yeast-Escherichia coli shuttle vectors constructed with in vitro mutagenized yeast genes lacking six-base pair restriction sites. *Gene*, **74**, 527–534.

32. Viscardi,V., Bonetti,D., Cartagena-Lirola,H., Lucchini,G. and Longhese,M.P. (2007) MRX-dependent DNA damage response to short telomeres. *Mol. Biol. Cell*, **18**, 3047–3058.

33. Lee,S.E., Moore,J.K., Holmes,A., Umezu,K., Kolodner,R.D. and Haber,J.E. (1998) Saccharomyces Ku70, Mre11/Rad50 and RPA proteins regulate adaptation to G2/M arrest after DNA damage. *Cell*, **94**, 399–409.

34. Pellicioli,A., Lee,S.E., Lucca,C., Foiani,M. and Haber,J.E. (2001) Regulation of Saccharomyces Rad53 checkpoint kinase during adaptation from DNA damage-induced G2/M arrest. *Mol. Cell*, **7**, 293–300.

35. Mantiero,D., Clerici,M., Lucchini,G. and Longhese,M.P. (2007) Dual role for Saccharomyces cerevisiae Tel1 in the checkpoint response to double-strand breaks. *EMBO Rep.*, **8**, 380–387.

36. Paciotti,V., Clerici,M., Lucchini,G. and Longhese,M.P. (2000) The checkpoint protein Ddc2, functionally related to S. pombe Rad26, interacts with Mec1 and is regulated by Mec1-dependent phosphorylation in budding yeast. *Genes Dev.*, **14**, 2046–2059.

37. Zhao,X., Muller,E.G. and Rothstein,R. (1998) A suppressor of two essential checkpoint genes identifies a novel protein that negatively affects dNTP pools. *Mol. Cell*, **2**, 329–340.

38. Redon,C., Pilch,D.R., Rogakou,E.P., Orr,A.H., Lowndes,N.F. and Bonner,W.M. (2003) Yeast histone 2A serine 129 is essential for the efficient repair of checkpoint-blind DNA damage. *EMBO Rep*, **4**, 678–684.

39. Nakada,D., Shimomura,T., Matsumoto,K. and Sugimoto,K. (2003). The ATM-related Tel1 protein of Saccharomyces cerevisiae controls a checkpoint response following phleomycin treatment. *Nucleic Acids Res.*, **31**, 1715–1724.

40. Ohle,C., Tesorero,R., Schermann,G., Dobrev,N., Sinning,I. and Fischer,T. (2016) Transient RNA-DNA hybrids are required for efficient double-strand break repair. *Cell*, **167**, 1001–1013.

41. Li,L., Germain,D.R., Poon,H.Y., Hildebrandt,M.R., Monckton,E.A., McDonald,D., Hendzel,M.J. and Godbout,R. (2016) DEAD Box 1 facilitates removal of RNA and homologous recombination at DNA double-strand breaks. *Mol. Cell. Biol.*, **36**, 2794–2810.

42. Hegnauer,A.M., Hustedt,N., Shimada,K., Pike,B.L., Vogel,M., Amsler,P., Rubin,S.M., van Leeuwen,F., Guénolé,A., van Attikum,H. *et al.* (2012) An N-terminal acidic region of Sgs1 interacts with Rpa70 and recruits Rad53 kinase to stalled forks. *EMBO J.*, **31**, 3768–3783.

43. Clerici,M., Mantiero,D., Lucchini,G. and Longhese,M.P. (2005) The Saccharomyces cerevisiae Sae2 protein promotes resection and bridging of double strand break ends. *J. Biol. Chem.*, **280**, 38631–38638.

44. Manfrini,N., Trovesi,C., Wery,M., Martina,M., Cesena,D., Descrimes,M., Morillon,A., d'Adda di Fagagna,F. and Longhese,M.P. (2015) RNA-processing proteins regulate Mec1/ATR activation by promoting generation of RPA-coated ssDNA. *EMBO Rep.*, **16**, 221–231.

45. Shima,H., Suzuki,M. and Shinohara,M. (2005) Isolation and characterization of novel xrs2 mutations in Saccharomyces cerevisiae. *Genetics*, **170**, 71–85.

46. Mimitou,E.P. and Symington,L.S. (2008) Sae2, Exo1 and Sgs1 collaborate in DNA double-strand break processing. *Nature*, **455**, 770–774.

47. Zhu,Z., Chung,W.H., Shim,E.Y., Lee,S.E. and Ira,G. (2008) Sgs1 helicase and two nucleases Dna2 and Exo1 resect DNA double-strand break ends. *Cell*, **134**, 981–994.

48. Gobbini,E., Villa,M., Gnugnoli,M., Menin,L., Clerici,M. and Longhese,M.P. (2015) Sae2 Function at DNA Double-Strand Breaks Is Bypassed by Dampening Tel1 or Rad53 Activity. *PLoS Genet.* **11**, e1005685.

49. Longhese,M.P., Plevani,P. and Lucchini,G. (1994) Replication factor A is required in vivo for DNA replication, repair, and recombination. *Mol Cell Biol.* **14**, 7884–7890.

50. Clerici,M., Mantiero,D., Lucchini,G. and Longhese,M.P. (2006) The Saccharomyces cerevisiae Sae2 protein negatively regulates DNA damage checkpoint signalling. *EMBO Rep.*, **7**, 212–218.

51. Giannattasio,M., Follonier,C., Tourrière,H., Puddu,F., Lazzaro,F., Pasero,P., Lopes,M., Plevani,P. and Muzi-Falconi,M. (2010) Exo1 competes with repair synthesis, converts NER intermediates to long ssDNA gaps, and promotes checkpoint activation. *Mol. Cell*, **40**, 50–62.

52. Baejen,C., Torkler,P., Gressel,S., Essig,K., Söding,J. and Cramer,P. (2014) Transcriptome maps of mRNP biogenesis factors define pre-mRNA recognition. *Mol. Cell*, **55**, 745–757.

53. Hurowitz,E.H. and Brown,P.O. (2003) Genome-wide analysis of mRNA lengths in Saccharomyces cerevisiae. *Genome Biol.*, **5**, R2.

54. Burkard,K.T. and Butler,J.S. (2000) A nuclear 3′-5′ exonuclease involved in mRNA degradation interacts with Poly(A) polymerase and the hnRNA protein Npl3p. *Mol. Cell. Biol.*, **20**, 604–616.

55. Nakada,D., Hirano,Y. and Sugimoto,K. (2004) Requirement of the Mre11 complex and exonuclease 1 for activation of the Mec1 signaling pathway. *Mol. Cell. Biol.*, **24**, 10016–10025.

56. Zierhut,C. and Diffley,J.F. (2008) Break dosage, cell cycle stage and DNA replication influence DNA double strand break response. *EMBO J.*, **27**, 1875–1885.

57. Lee,M.S., Henry,M. and Silver,P.A. (1996) A protein that shuttles between the nucleus and the cytoplasm is an important mediator of RNA export. *Genes Dev.*, **10**, 1233–1246.

58. Libri,D., Dower,K., Boulay,J., Thomsen,R., Rosbash,M. and Jensen,T.H. (2002) Interactions between mRNA export commitment, 3′-end quality control, and nuclear degradation. *Mol. Cell. Biol.*, **22**, 8254–8266.

59. Hilleren,P., McCarthy,T., Rosbash,M., Parker,R. and Jensen,T.H. (2001) Quality control of mRNA 3′-end processing is linked to the nuclear exosome. *Nature*, **413**, 538–542.

60. Kallehauge,T.B., Robert,M.C., Bertrand,E. and Jensen,T.H. (2012) Nuclear retention prevents premature cytoplasmic appearance of mRNA. *Mol. Cell*, **48**, 145–152.

61. Babour,A., Shen,Q., Dos-Santos,J., Murray,S., Gay,A., Challal,D., Fasken,M., Palancade,B., Corbett,A., Libri,D. *et al.* (2016) The Chromatin Remodeler ISW1 Is a Quality Control Factor that Surveys Nuclear mRNP Biogenesis. *Cell*, **167**, 1201–1214.

62. Tran,P.T., Erdeniz,N., Dudley,S. and Liskay,R.M. (2002) Characterization of nuclease-dependent functions of Exo1p in Saccharomyces cerevisiae. *DNA Repair (Amst)*, **1**, 895–912.

63. Cotta-Ramusino,C., Fachinetti,D., Lucca,C., Doksani,Y., Lopes,M., Sogo,J. and Foiani,M. (2005) Exo1 processes stalled replication forks and counteracts fork reversal in checkpoint-defective cells. *Mol. Cell*, **17**, 153–159.

64. Maringele,L. and Lydall,D. (2002) EXO1-dependent single-stranded DNA at telomeres activates subsets of DNA damage and spindle checkpoint pathways in budding yeast yku70Delta mutants. *Genes Dev.*, **16**, 1919–1933.

65. Tsubouchi,H. and Ogawa,H. (2000) Exo1 roles for repair of DNA double-strand breaks and meiotic crossing over in Saccharomyces cerevisiae. *Mol. Biol. Cell*, **11**, 2221–2233.

66. Savage,K.I., Gorski,J.J., Barros,E.M., Irwin,G.W., Manti,L., Powell,A.J., Pellagatti,A., Lukashchuk,N., McCance,D.J., McCluggage,W.G. *et al.* (2014) Identification of a BRCA1-mRNA splicing complex required for efficient DNA repair and maintenance of genomic stability. *Mol. Cell*, **54**, 445–459.